Site-specific backbone amide ^{15}N chemical shift anisotropy tensors from liquid crystal and cross-correlated relaxation measurements

Laboratory of Chemical Physics, NIDDK, National Institutes of Health, Bethesda, MD 20892-0520

Lishan Yao,[a] Alexander Grishaev,[a] Gabriel Cornilescu[b] and Ad Bax[a]
[a] Laboratory of Chemical Physics, NIDDK
National Institutes of Health, Bethesda, MD 20892-0520
[b] National Magnetic Resonance Facility, Madison, WI 53706

SUPPORTING INFORMATION

Data Analysis

Site specific relaxation rates for amide ^{15}N were calculated from the CSA, dipole-dipole interaction, rotational diffusion tensor and structure using the following equations:

$$R_1 = R_1^{CSA} + \sum_{r<4\text{A}} R_1^{DD} \tag{1a}$$

$$R_2 = R_2^{CSA} + \sum_{r<4\text{A}} R_2^{DD} \tag{1b}$$

where the summation includes ^{13}C', ^{13}C$^{\alpha}$, ^{2}H and ^{1}H nuclei within a 4Å radius from the ^{15}N nucleus considered. The CSA contribution is calculated as:

$$R_1^{CSA} = \omega_N^2 G\left(\omega_N, CSA, D_{XX}, D_{YY}, D_{ZZ}, \alpha, \beta, \gamma\right) \tag{2a}$$

$$R_2^{CSA} = \frac{\omega_N^2}{6}\left\{4G\left(0, CSA, D_{XX}, D_{YY}, D_{ZZ}, \alpha, \beta, \gamma\right) + 3G\left(\omega_N, CSA, D_{XX}, D_{YY}, D_{ZZ}, \alpha, \beta, \gamma\right)\right\} \tag{2b}$$

where ω_N is the ^{15}N nuclear angular frequency, D_{XX}, D_{YY}, D_{ZZ} are the eigenvalues of the rotational diffusion tensor ($D_{ZZ} \geq D_{YY} \geq D_{XX}$) and α, β, γ are the Euler angles (z-y-z convention)[1] for rotating the CSA principal axes to the diffusion tensor principal axis system. The function G is written as:

$$G\left(\omega, CSA, D_{XX}, D_{YY}, D_{ZZ}, \alpha, \beta, \gamma\right) = \sum_{i=1}^{5} \frac{S^2 c_i \tau_i}{1 + \omega^2 \tau_i^2} \tag{3}$$

$$c_1 = \frac{1}{40}\left\{3\sin^2\beta\sin 2\gamma - \eta_\lambda\left[\cos 2\alpha \sin 2\gamma\left(1+\cos^2\beta\right) + 2\sin 2\alpha\cos\beta\cos 2\gamma\right]\right\}^2 \Delta_\lambda^2$$

$$c_2 = \frac{1}{40}\left\{3\sin 2\beta\cos\gamma + \eta_\lambda\left[\cos 2\alpha\sin 2\beta\cos\gamma - 2\sin 2\alpha\sin\beta\sin\gamma\right]\right\}^2 \Delta_\lambda^2$$

$$c_3 = \left\{\begin{array}{l} 1.5(1+A)\left(3\cos^2\beta - 1 - \eta_\lambda\sin^2\beta\cos 2\alpha\right) - 0.5\eta_D \\ \times\left[3\sin^2\beta\cos 2\gamma - \eta_\lambda\left(\cos 2\alpha\cos 2\gamma(1+\cos^2\beta) - 2\sin 2\alpha\cos\beta\sin 2\gamma\right)\right] \end{array}\right\}^2 \frac{\Delta_\lambda^2}{60A(1+A)}$$

$$c_4 = \frac{1}{40}\left\{3\sin 2\beta\sin\gamma + \eta_\lambda\left[\cos 2\alpha\sin 2\beta\sin\gamma + 2\sin 2\alpha\sin\beta\cos\gamma\right]\right\}^2 \Delta_\lambda^2$$

$$c_5 = \left\{\begin{array}{l} -0.5\eta_D\left(3\cos^2\beta - 1 - \eta_\lambda\sin^2\beta\cos 2\alpha\right) + 0.5(1+A) \\ \times\left[3\sin^2\beta\cos 2\gamma - \eta_\lambda\left(\cos 2\alpha\cos 2\gamma(1+\cos^2\beta) - 2\sin 2\alpha\cos\beta\sin 2\gamma\right)\right] \end{array}\right\}^2 \frac{\Delta_\lambda^2}{20A(1+A)}$$

$$\tau_1 = \frac{1}{6D_S\left(1 + \frac{D^*}{2D_S}\right)}$$

$$\tau_2 = \frac{1}{6D_S\left(1 - \frac{D^*(1-\eta_D)}{4D_S}\right)}$$

$$\tau_3 = \frac{1}{6D_S\left(1 - \frac{D^*A}{2D_S}\right)}$$

$$\tau_4 = \frac{1}{6D_S\left(1-\frac{D^*(1+\eta_D)}{4D_S}\right)}$$

$$\tau_5 = \frac{1}{6D_S\left(1+\frac{D^*A}{2D_S}\right)}$$

where

$$\Delta_\lambda = \sigma_{ZZ}$$

$$\eta_\lambda = \frac{\sigma_{YY}-\sigma_{XX}}{\sigma_{ZZ}}$$

$$A = \sqrt{1+\frac{\eta_D^2}{3}}$$

$$D_S = \frac{D_{XX}+D_{YY}+D_{ZZ}}{3}$$

$$D^* = D_{ZZ} - D_S$$

$$\eta_D = \frac{D_{YY}-D_{XX}}{D^*} \; (\eta_D = 0 \text{ if } D^* = 0)$$

The dipole-dipole contribution to the relaxation rate is calculated by

$$R_1^{DD} = \frac{4I(I+1)}{9}\xi^2\left\{\begin{array}{l}3G(\omega_N, DD, D_{XX}, D_{YY}, D_{ZZ}, \alpha, \beta, \gamma) + G(\omega_N - \omega_X, DD, D_{XX}, D_{YY}, D_{ZZ}, \alpha, \beta, \gamma) \\ + 6G(\omega_N + \omega_X, DD, D_{XX}, D_{YY}, D_{ZZ}, \alpha, \beta, \gamma)\end{array}\right\} \tag{4a}$$

$$R_2^{DD} = \frac{2I(I+1)}{9}\xi^2\left\{\begin{array}{l}4G(0, DD, D_{XX}, D_{YY}, D_{ZZ}, \alpha, \beta, \gamma) + 3G(\omega_N, DD, D_{XX}, D_{YY}, D_{ZZ}, \alpha, \beta, \gamma) \\ + G(\omega_N - \omega_X, DD, D_{XX}, D_{YY}, D_{ZZ}, \alpha, \beta, \gamma) + 6G(\omega_X, DD, D_{XX}, D_{YY}, D_{ZZ}, \alpha, \beta, \gamma) \\ + 6G(\omega_N + \omega_X, DD, D_{XX}, D_{YY}, D_{ZZ}, \alpha, \beta, \gamma)\end{array}\right\} \tag{4b}$$

where I is the nuclear spin angular momentum quantum number (1/2 for ^{1}H, ^{15}N, ^{13}C and 1 for ^{2}H). $\xi = \frac{-\mu_0\hbar\gamma_N\gamma_X}{4\pi r_{eff}^3}$. G(DD) has the same form as G(CSA) except that $\sigma_{XX} = \sigma_{YY} = -0.5\sigma_{ZZ} = -0.5$ with σ_{ZZ} parallel to the dipole vector (z axis). As a result η_λ equals zero. The Euler angles α, β, γ (z-y-z convention) describe the rotation from the dipole-dipole principal axis system to that of the diffusion tensor. The ^{15}N CSA and N-H (or N-C') dipole cross-correlated relaxation rate are calculated by

$$\Gamma = \frac{R_2^{C+D} - R_2^{C-D}}{2} \tag{5}$$

where $R_2^{C\pm D}$ has the same form as R_2^{CSA} (eq 2b) except that the CSA in $R_2^{C\pm D}$ equation is a pseudo-CSA defined by the sum (for C+D) and difference (for C–D) of DD and CSA tensors. The sum (or difference) of dipole-dipole and CSA tensors is calculated using equation

$$\sigma_{C\pm D} = \sigma \pm \varepsilon R \zeta R^T \quad (6)$$

where $\sigma = \begin{Bmatrix} \sigma_{XX} & 0 & 0 \\ 0 & \sigma_{YY} & 0 \\ 0 & 0 & \sigma_{ZZ} \end{Bmatrix}$, $\zeta = \begin{Bmatrix} -0.5 & 0 & 0 \\ 0 & -0.5 & 0 \\ 0 & 0 & 1 \end{Bmatrix}$, $\varepsilon = \xi / \omega_N$, $R = V_C{}^T V_D$. V_C and V_D are matrices defining the principal axes (as column vectors) of CSA and DD tensors and the superscript ^{T} denotes the transpose operation. To proceed further, $\sigma_{C\pm D}$ needs to be diagonalized, so that $\sigma_{C\pm D}^{diag} = V_\pm^T \sigma_{C\pm D} V_\pm$, with the principal axes defined by matrix (as column vectors) $V_{C\pm D} = V_C V_\pm$. Note that Vc rotates the axes from the molecular frame to the CSA principal axis frame, $V_\pm$ rotates the axes from the CSA principal axis frame to the CSA±D frame. So the total rotation, $VcV_\pm$, defines the principal axes of the CSA±D tensor. R_2 relaxation rates resulting from this pseudo CSA can then be calculated using equations 2b and 5 above.

For each residue, three parameters, $\Delta\sigma$ defined as $\sigma_{ZZ} - (\sigma_{XX} + \sigma_{YY})/2$ (with $|\sigma_{ZZ}| \geq |\sigma_{XX}| \geq |\sigma_{YY}|$), the asymmetry parameter η, defined as $(\sigma_{YY} - \sigma_{XX})/\sigma_{ZZ}$, and the angle β between the least shielded σ_{ZZ} axis and the N-H bond are fitted against ten experimental numbers, including the ^{15}N RCSAs under six different alignment orientations, the ^{15}N CSA/N-H and ^{15}N CSA/N-C' cross-correlated transverse relaxation rates, and the R_1 rates of the ^{15}N-^{2}H groups at two magnetic fields, corresponding to 600 and 800 MHz ^{1}H frequencies. Two global parameters, a uniform order parameter $\boldsymbol{S}^2$ and the tumbling time τ_c (defined as $1/6D_S$), are also included in the fitting. The fitting was performed in the following way,

1. An initial value for τ_c in D_2O at 283 K was set to 6.0 ns, based on the viscosity difference between D_2O and H_2O and the temperature (283 K) at which data were collected.
2. The CSA tensor was fitted to minimize the χ^2 value for each residue and a global $\boldsymbol{S}^2$ value was simultaneously optimized to minimize the total χ^2.
3. The τ_c value was then adjusted such that the slope of the best fitting line between the predicted and experimental R_2 value of ^{15}N-^{2}H moieties equals 1.
4. Repeat step 2 and monitor the experimental and fitted R_2 rates so that no systematic bias remains.

The optimum τ_c and $\boldsymbol{S}^2$ values obtained in this manner are 6.63 ns and 0.903, respectively. The optimized CSA tensors are listed in Table S3. The errors were determined from 100 Monte Carlo simulations with Gaussian noise (defined by experimental errors) during which the τ_c and $\boldsymbol{S}^2$ values are kept fixed at 6.63 ns and 0.903.

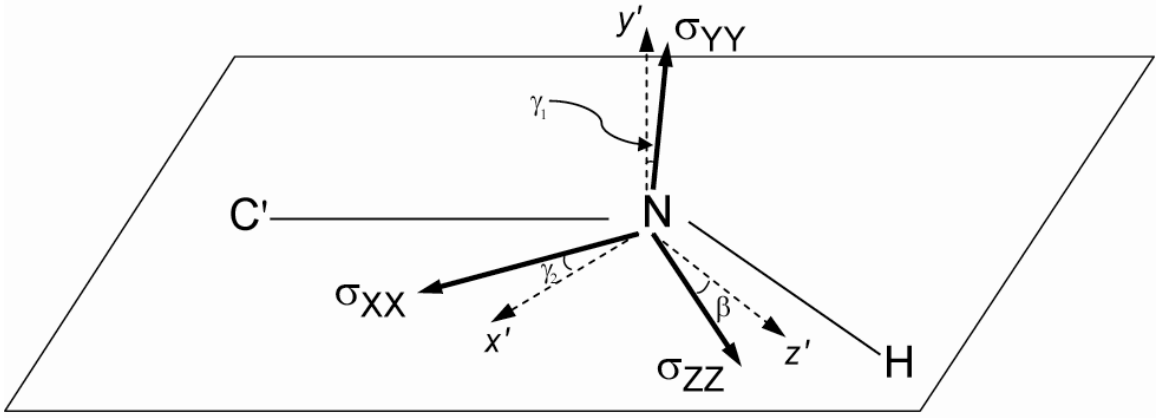

Scheme S1. The coordinate system and angles used to describe the orientation of the CSA tensor. The *y′* axis is orthogonal to the plane defined by C'-N-H, while the x' and z' axes are in this plane, with z' parallel to the N-H bond vector. The angle between the *z′* axis and σ_{ZZ} is defined as β (with left-handed rotation about the *y′* axis defined as positive); the angle between σ_{YY} and the *y′* axis is defined as γ_1 (with left-handed rotation about the *x′* axis being positive); the angle between σ_{XX} and *x′* axis is defined as γ_2 (with left-handed rotation about *z′* being positive).

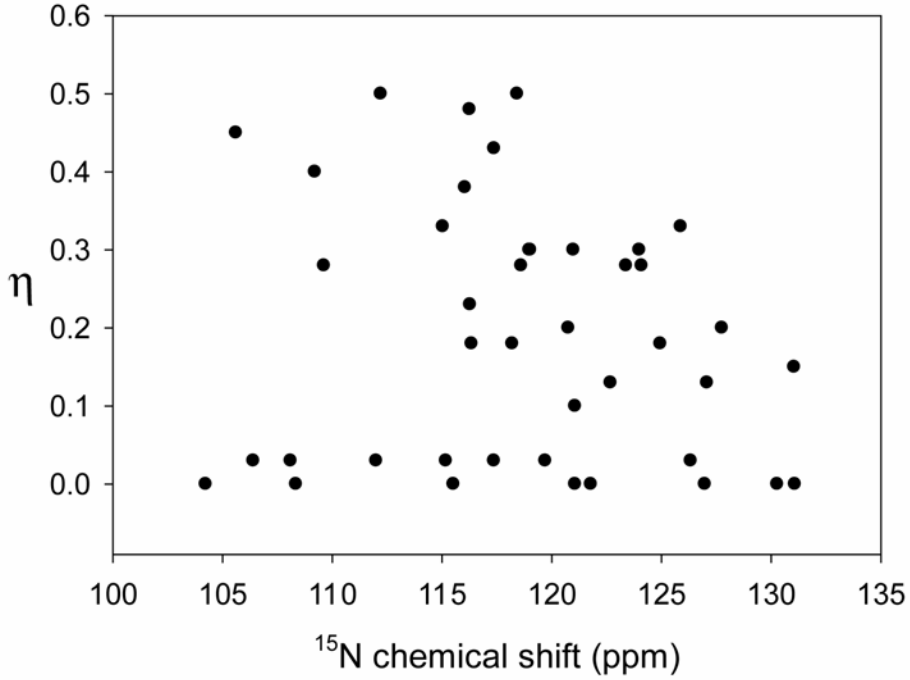

Figure S1. Correlation between the ^{15}N CSA asymmetry parameter, η, of protein GB1 derived by slow MAS spinning solid state NMR[2] and the ^{15}N isotropic chemical shift observed in the microcrystalline GB1 sample (BMRB entry 15156). $\eta = (\sigma_{YY} - \sigma_{XX})/\sigma_{ZZ}$.

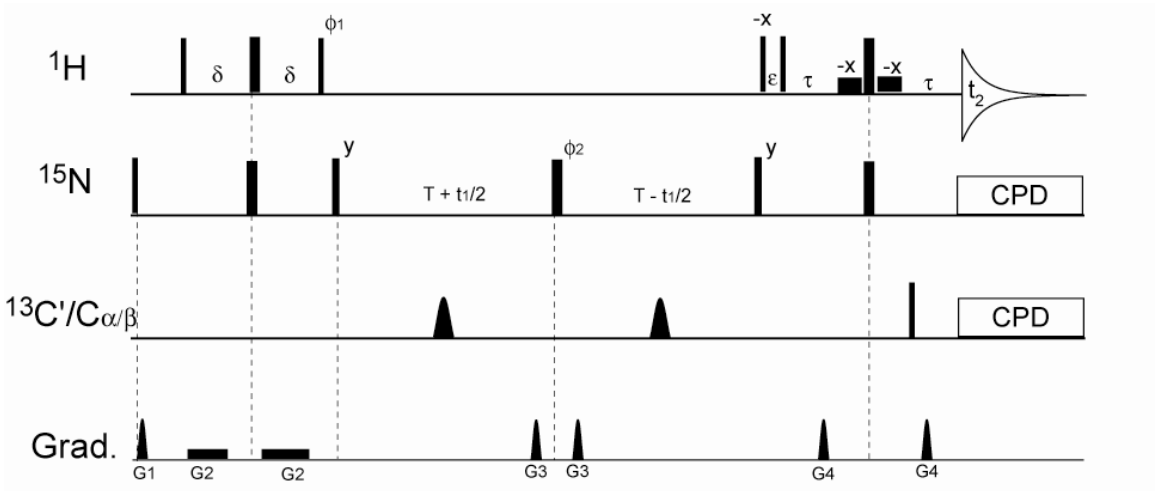

Figure S2. Pulse sequence used to measure the ^{15}N CSA and ^{15}N-^{1}H dipole transverse cross-correlation rate, $\Gamma^{CSA,NH}$. Narrow and wide pulses correspond to 90º and 180º flip angles, respectively. The two low power pulses immediately preceding and following the last nonselective ^{1}H 180º pulse have a width of 1 ms each and correspond to flip angles of 90º as part of the WATERGATE water suppression scheme. All the ^{1}H pulses are centered on the H_2O resonance, at 4.77 ppm. The ^{13}C'/$C_{\alpha/\beta}$ nuclei are decoupled by two 0.6 ms hyperbolic secant pulses, centered at 116.8 ppm and covering a bandwidth of ±13 kHz. The phases of all pulses are *x* unless indicated. δ = 2.6 ms, τ = 1.6 ms. T was set to 40.8 ms at 500 MHz and to 40.8 and 80.8 ms at 600 MHz; ε = 0.132 ms at 500 MHz and 0.111 ms at 600 MHz. Phase cycling: ϕ_1 = 4(*y*), 4(-*y*); ϕ_2 = *x*, *y*, -*x*, -*y*; Rec. = *x*, -*x*, *x*, -*x*, -*x*, *x*, -*x*, *x*. Pulsed field gradients $G_{1,3,4}$ are sine-bell shaped with maximum gradient strengths at their midpoints of 7.2 G/cm, 21.0 G/cm and -9.0 G/cm respectively. G_2 is rectangular shaped pulse with a strength of 0.6 G/cm. The durations for gradient pulses are $G_{1,2,3,4}$ = 0.75, 2.6, 0.1, 0.7 ms. All gradient pulses are applied along the *z* axis.

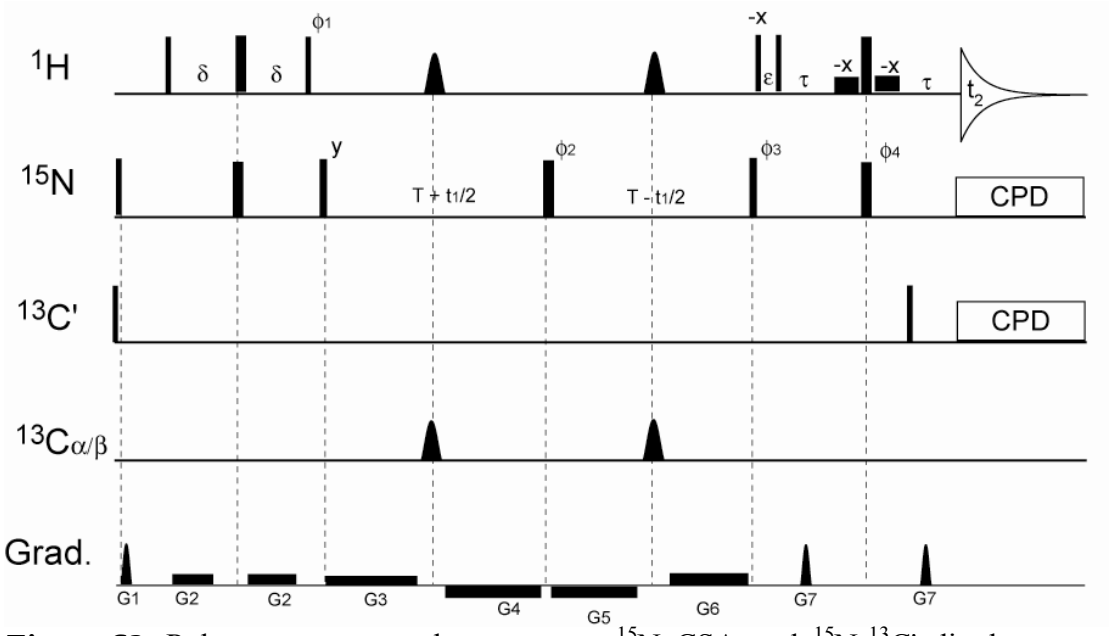

Figure S3. Pulse sequence used to measure ^{15}N CSA and ^{15}N-^{13}C' dipole transverse cross-correlated relaxation rate $\Gamma^{CSA,NC'}$. Narrow and wide pulses correspond to 90º and 180º flip angles, respectively. The two low power pulses immediately preceding and following the last nonselective ^{1}H 180º pulse have a duration of 1 ms each and correspond to flip angles of 90º as part of the WATERGATE water suppression scheme. All ^{1}H pulses are centered on water, at 4.77 ppm. Two hyperbolic secant pulses are employed to decouple the amide protons (with durations of 0.6 ms at 500 MHz and 0.5 ms at 600 MHz; centered at 4.77 ppm and covering ±13 kHz (0.6ms) or ±16 kHz (0.5ms)) during ^{15}N evolution. Weak gradient pulses G_4 and G_5 are applied to maintain the water along $-z$ in between the ^{1}H inversion pulses. The $^{13}C_{\alpha/\beta}$ nuclei are decoupled by two 2 ms hyperbolic secant pulses (centered at 56.7 ppm and covering ±3.9 kHz). The phases of all pulses are x unless indicated. T = 82.55 ms, δ = 2.6 ms, τ = 1.6 ms and ε = 0.132 ms at 500 MHz and 0.111 ms at 600 MHz. $\phi_1 = 4(y), 4(-y)$; $\phi_2 = x, y$; $\phi_3 = 2(y), 2(-y)$; $\phi_4 = 8(x), 8(-x)$; and Rec. = x, $-x$, $-x$, x, $-x$, x, x, $-x$. Pulsed field gradients G_1 and G_7 are sine-bell shaped with maximum gradient strengths at their midpoints of 16.2 G/cm and 7.2 G/cm respectively. $G_{2,3,4,5,6}$ are rectangular shaped pulses with the strengths of 0.6 G/cm for G_2, 0.3 G/cm for G_3, -0.3 G/cm for G_4, -0.3 G/cm for G_5 and 0.3 G/cm for G_6. The durations for gradient pulses are $G_{1,2,3,4,5,6,7}$ = 0.75 ms, 2.6 ms, T/2-t_1/4, T/2-t_1/4, T/2+t_1/4, T/2+t_1/4, 0.7 ms. All gradient pulses are applied along the z axis.

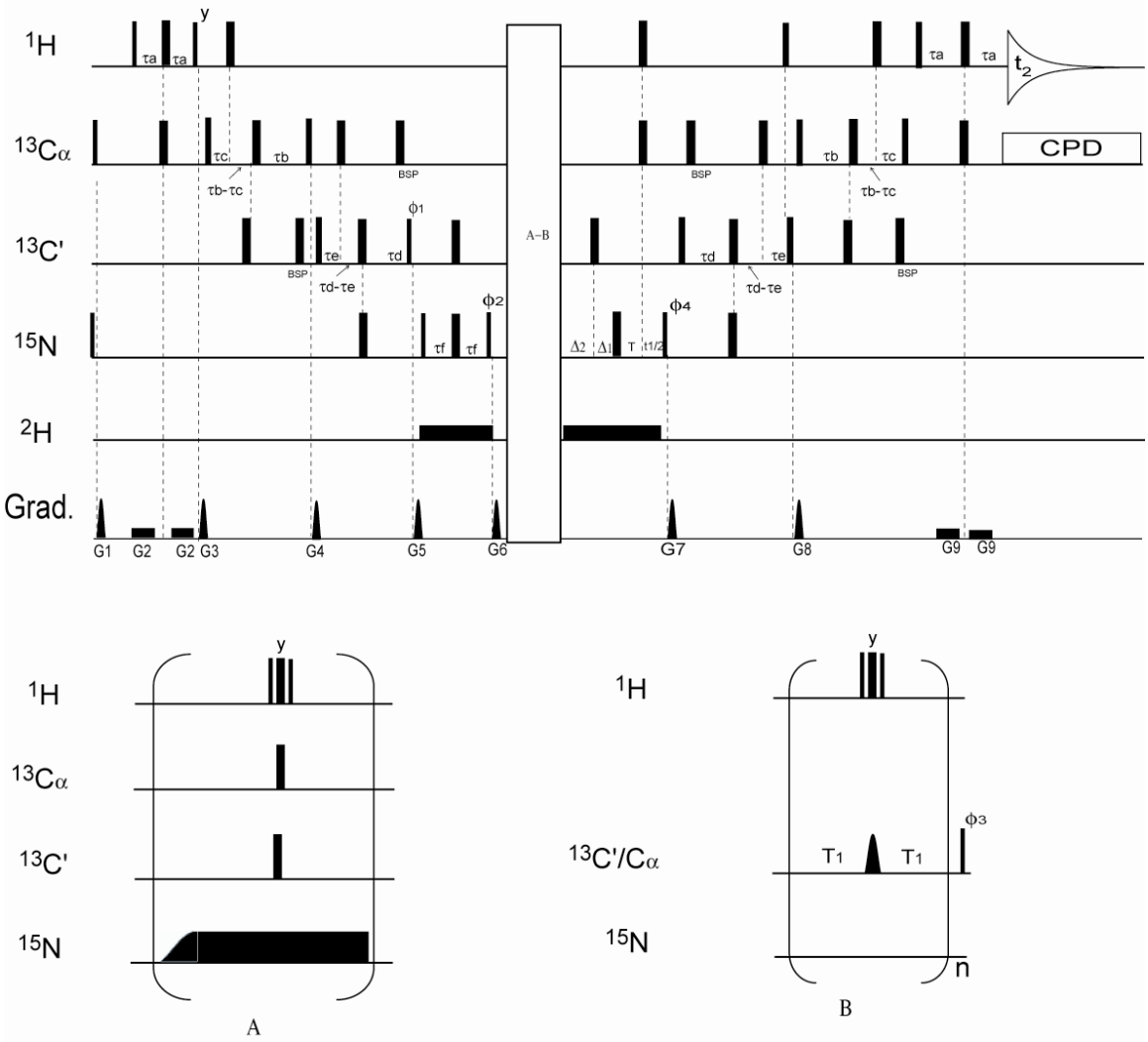

Figure S4. The HA(CACO)N pulse sequence used to measure ^{15}N $R_{1\rho}$ (A) and R_1 (B) relaxation rates of ^{15}N-^{2}H groups, adapted from reference 3.[3] Narrow and wide pulses correspond to 90º and 180º flip angles, respectively. The phase of all pulses is *x* unless indicated. All ^{1}H pulses are centered on the HDO resonance, at 4.75 ppm. CW ^{2}H decoupling with an RF field strength of 417 Hz was applied with the ^{2}H carrier set to 8.6 ppm to remove the ^{15}N-^{2}H J coupling. Pulses marked "BSP" compensate for Bloch-Siegert induced phase shifts. In the spin-lock $R_{1\rho}$ experiment (A), $^{15}N_z$ magnetization was tilted to the *x*-*z* plane by means of a 3ms half-hyperbolic secant pulse and then spin-locked by a rectangular pulse with a field strength of 2.0 kHz. RF heating compensation pulses were applied at the beginning of each scan in order to keep the effect of RF heating constant during the entire experiment.[4] A proton composite 90º$_x$-210º$_y$-90º$_x$, a ^{13}C' 180º and a $^{13}C^{\alpha}$ 180º pulse were applied to suppress ^{15}N CSA/^{1}N-^{1}H, ^{15}N-^{13}C' and ^{15}N-$^{13}C^{\alpha}$ dipole cross-correlated relaxation effects. In the ^{15}N R_1 (B) experiment, a 0.5 ms hyperbolic secant 180º pulse and a proton composite 90º$_x$-210º$_y$-90º$_x$ pulse were applied for the same purpose. Delays used are $\tau_a = \tau_c = 1.6$ ms, $\tau_b = 3.0$ ms, $\tau_d = 14.5$ ms, $\tau_e = 4.5$ ms, $\tau_f = 16$ ms, T = 16 ms, $T_1 = 25$ms. Mixed-time t_1 evolution[5] is used to optimize ^{15}N resolution, with $\Delta_1 = \max(0, t_1/2\text{-}T)$, $\Delta_2 = \max(0, T\text{-}t_1/2)$. The phase cycling employed in

the R_1 experiment is $\phi_1 = x,-x$; $\phi_2 = 4(y), 4(-y)$; $\phi_3 = 2(x), 2(-x)$; $\phi_4 = y$, with Rec. = y, $-y$, $-y$, y, $-y$, y, y, $-y$. The phase cycling in the $R_{1\rho}$ experiment is $\phi_1 = x,-x$; $\phi_2 = 4(y), 4(-y)$; $\phi_4 = 2(x), 2(-x)$; and Rec. = y, $-y$, $-y$, y, $-y$, y, y, $-y$. Pulsed field gradients $G_{1,3,4,5,6,7,8}$ are sine-bell shaped with maximum gradient strengths at their midpoints of 16.2 G/cm for G_1, 3.6 G/cm for G_3, 7.8 G/cm for G_4, 10.2 G/cm for G_5, 19.8 G/cm for G_6, 9.0 G/cm for G_7 and 5.4 G/cm for G_8. $G_{2,9}$ are rectangular shaped pulses with strengths of 1.2 G/cm for G_2 and 3 G/cm for G_9. The durations for gradient pulses are $G_{1,2,3,4,5,6,7,8,9}$ = 1.0 , 1.6 , 1.0 , 1.0 , 1.0 , 1.0 , 1.0 , 1.0 , 1.6 ms. All gradient pulses are applied along the *z* axis.

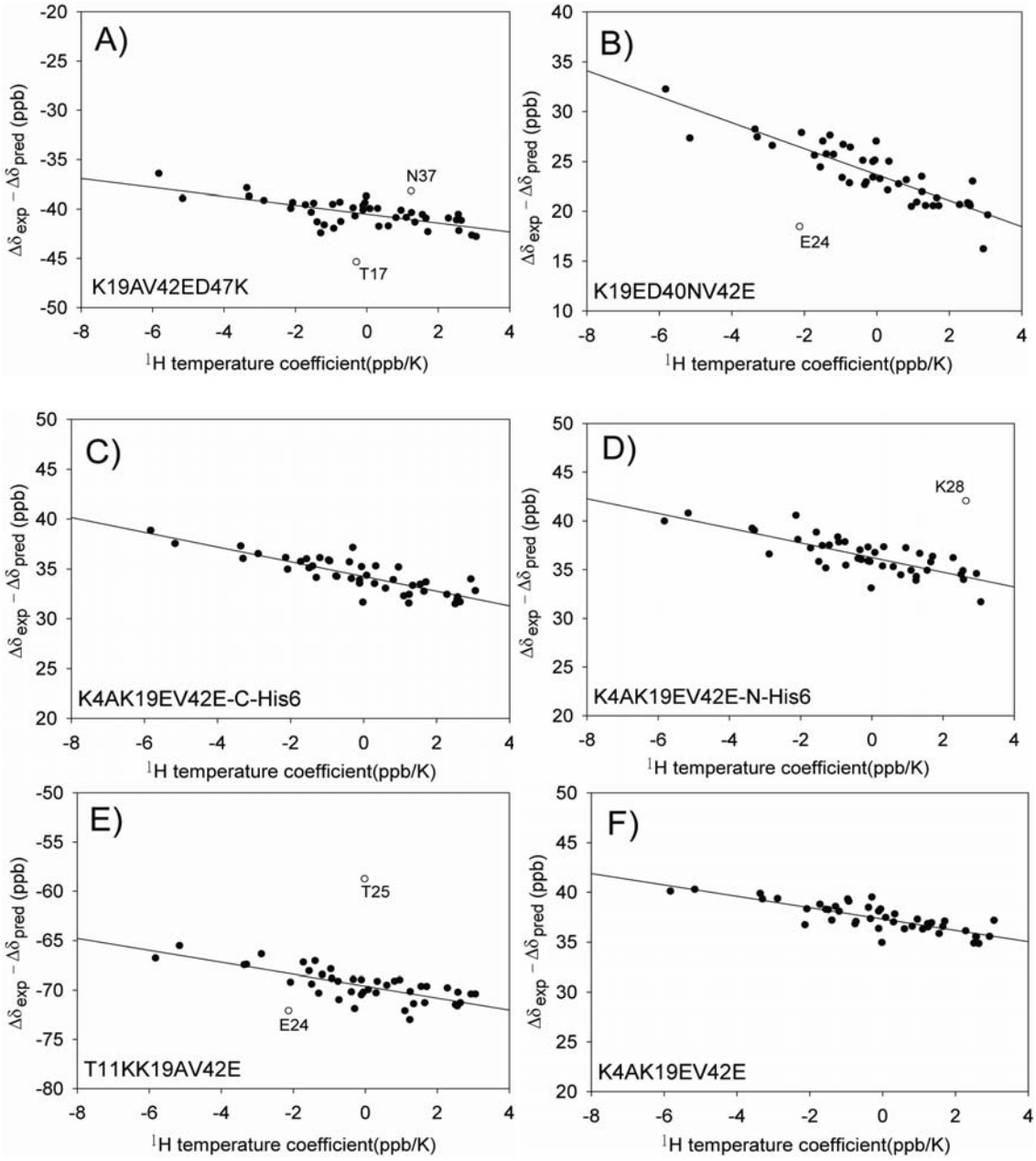

Figure S5. The correlation between $\Delta\delta_{exp} - \Delta\delta_{pred}$ of $^1H^N$ and the apparent ^1H chemical shift temperature coefficients (Table S1), where $\Delta\delta_{exp}$ is the experimental RCSA and $\Delta\delta_{pred}$ is the predicted RCSA based on the literature ^1H CSA value[6] and the alignment tensor determined from ^{15}N-^1H RDCs. The slopes and intercepts are listed in Table S2.

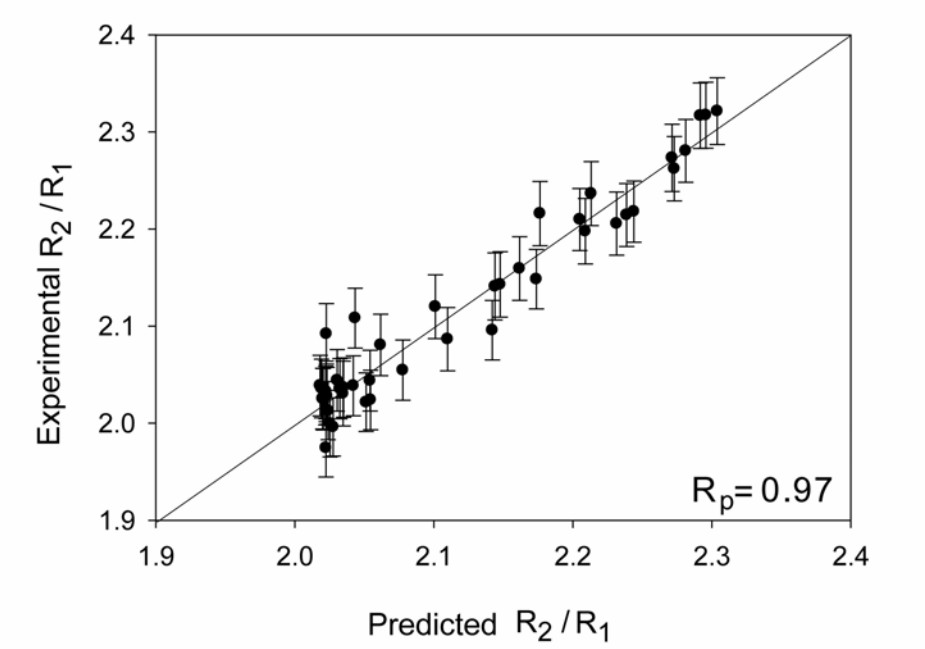

Figure S6. The correlation between experimental and predicted R_2/R_1 ratios, after optimization of the rotational diffusion tensor in determining the diffusion tensor of mutant K4AK19EV42E. The diffusion tensor values are listed in Table 2.

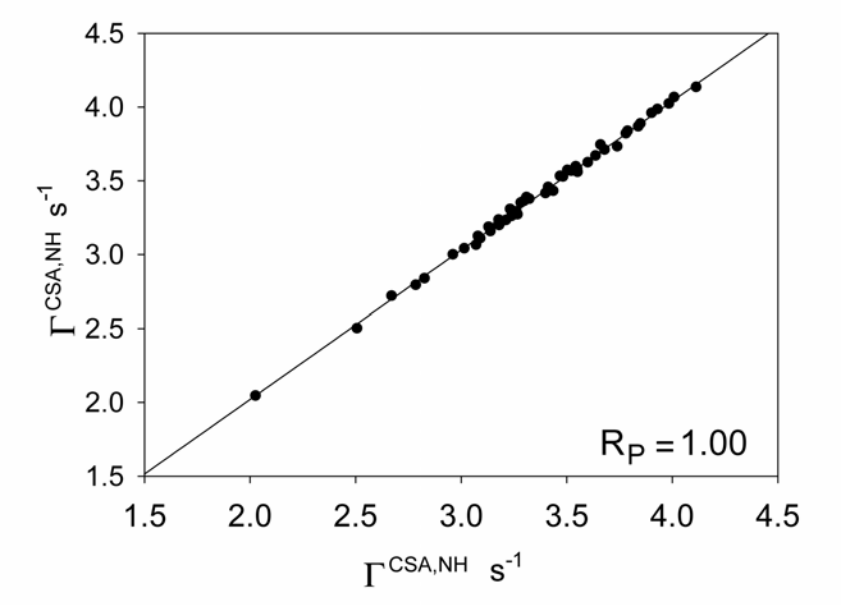

Figure S7. Comparison of $\Gamma^{CSA,NH}$ transverse cross-correlation rates measured using transverse evolution durations (2T in Figure S2) of 81.6 ms (x axis)and 161.6 ms (y axis). The best fitted slope is 1.01, with R_P = 1.0.

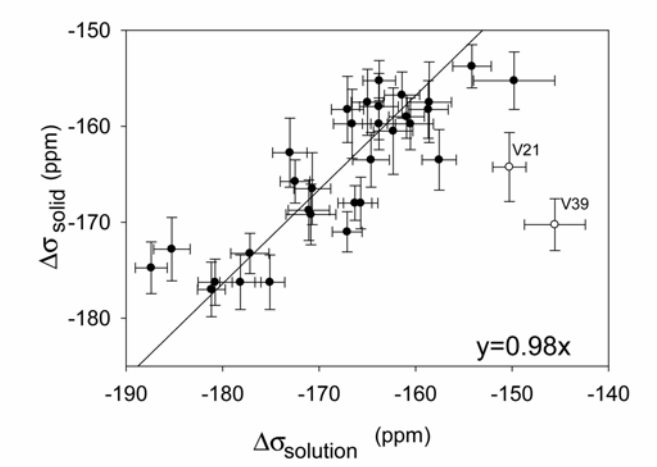

Figure S8. Correlation between ^{15}N CSA magnitude, Δσ, measured using solid state NMR for protein GB1[2] (y axis) and solution NMR in this work (x axis) for GB3. The correlation coefficient R_P is 0.77 after excluding two outliers V21 and V39.

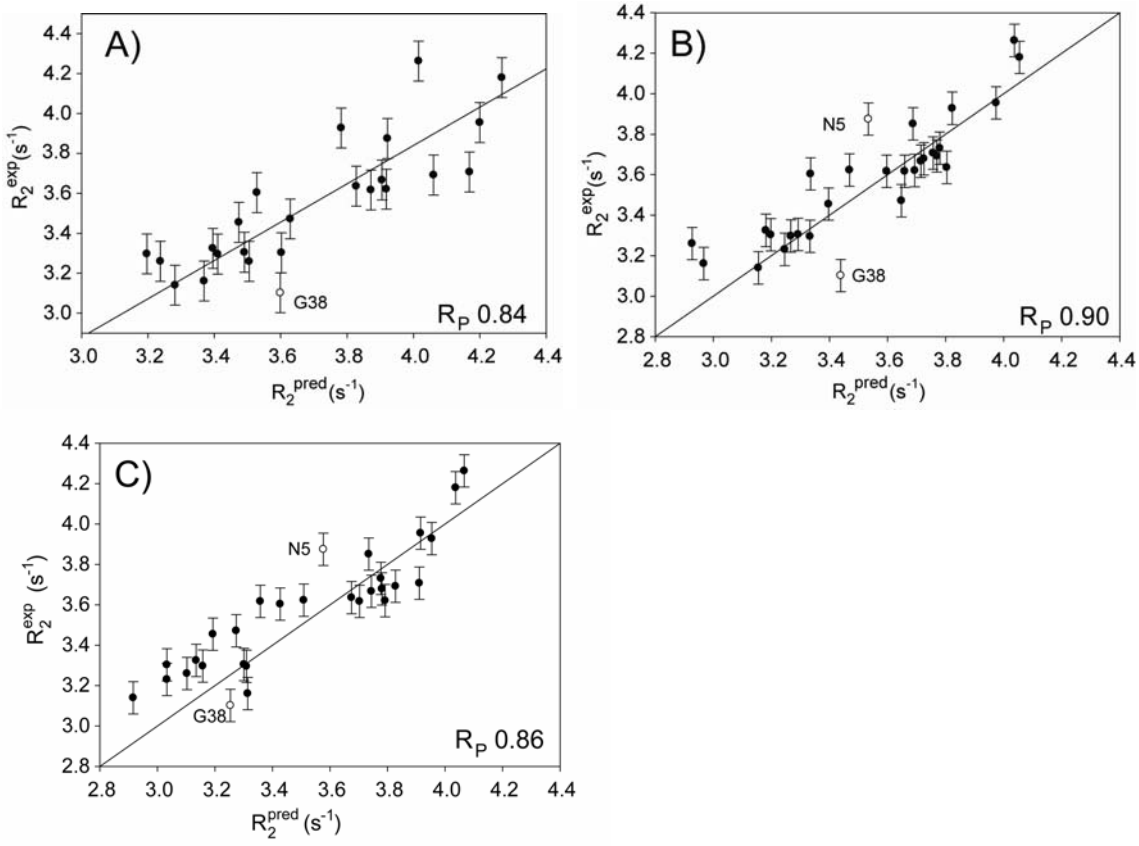

Figure S9. Correlation between experimental and predicted R_2 rates of ^{15}N-{^2H} groups in GB3. The predicted rates were calculated using site-specific ^{15}N CSA (A) determined previously by solid state NMR,[2], (B) derived in this study but fixing β at 19.6º, and (C) with η = 0 but residue specific β value. The best fitted line has a slope of 0.96 (A), 1.01 (B), and 1.02 (C).

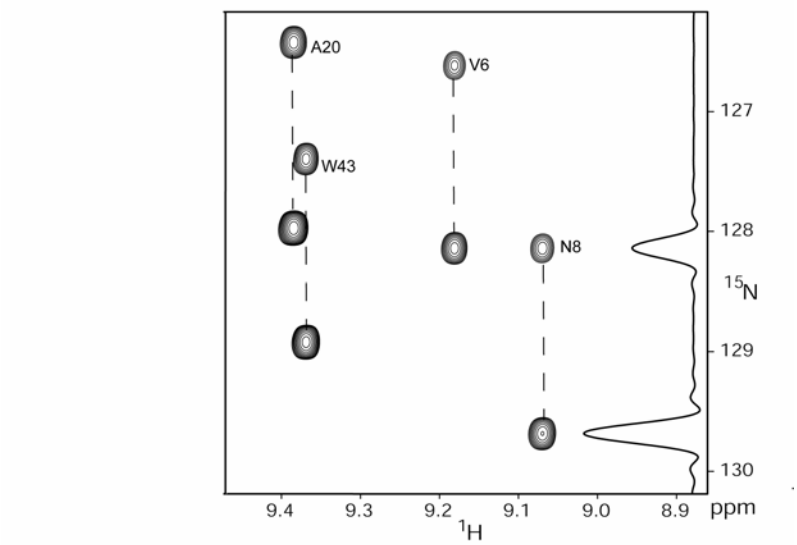

Figure S10. Small region of the ^{1}H-^{15}N HSQC spectrum recorded with a constant-time evolution period of 81.6 ms at 600 MHz ^{1}H frequency, in the absence of ^{1}H decoupling during ^{15}N evolution. The intensity ration of the ^{15}N-{^{1}H} doublet components yields the cross correlated relaxation rate, $\Gamma^{CSA,NH}$.

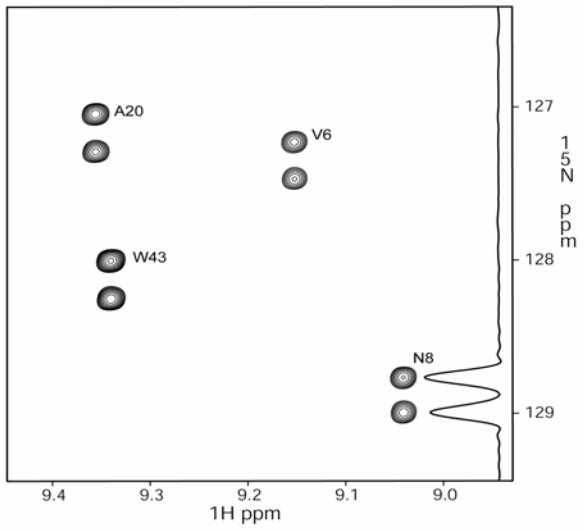

Figure S11. Small region of the ^{1}H-^{15}N HSQC spectrum recorded with a constant-time evolution period of 165.1 ms at 600 MHz ^{1}H frequency, in the absence of ^{1}H decoupling during ^{15}N evolution. The intensity ratio of the ^{15}N-{^{1}H} doublet components yields the cross correlated relaxation rate, $\Gamma^{CSA,NC'}$.

Table S1. Apparent temperature coefficients for amide ^{1}H, ^{15}N and carbonyl ^{13}C in GB3, which correspond approximately to the difference between the true temperature coefficients and the temperature coefficient of H_2O (-10.32 ppb/K).[7] Values were obtained from 3D HNCO experiments carried out at 298K and 306K for the mutant K19AV42ED47K, and the temperature coefficients were derived from the chemical shift differences divided by the temperature difference, leaving the apparent carrier frequency unchanged while locked on HDO, i.e., not accounting for the change in lock and reference frequency (in ppm) with temperature.

residue	^{1}H (ppb/K)	^{13}C (ppb/K)	^{15}N (ppb/K)
3	-2.87	3.50	-21.84
4	-0.38	5.44	4.18
5	1.26	3.83	6.66
6	-0.72	2.31	-2.78
7	0.31	4.41	0.63
8	0.61	1.44	1.79
9	-1.28	-2.91	-16.96
10	-1.26	5.90	-1.87
11	-1.37	-0.77	3.54
12	-2.96	2.94	-21.87
13	-4.65	5.22	-18.01
14	-0.20	-0.67	-6.50
15	-4.49	3.16	-7.26
16	1.11	3.76	5.49
17	-0.29	0.45	17.80
18	-0.10	4.65	-6.95
19	-0.04	14.15	3.10
20	-6.68	-1.49	-10.33
21	-3.35	-3.97	-2.56
22	2.58	5.70	5.87
23	-1.38	6.39	6.00
24	-2.12	1.61	-4.29
25	-0.01	-1.40	-5.68
26	0.82	0.20	-16.37
27	-1.55	1.43	-3.19
28	2.65	4.48	1.84
29	3.07	-1.37	-0.77
30	-0.75	-1.97	-13.06
31	0.34	3.50	-3.41
32	1.56	-0.84	-7.47

33	-0.10	6.36	-4.21
34	-1.19	-1.71	-5.43
35	2.29	2.87	-6.73
36	-1.71	-1.56	0.19
37	1.25	6.04	-3.91
38	1.66	6.92	-0.02
39	0.09	2.63	-5.41
40	-5.14	-0.13	-20.16
41	-2.12	4.70	-9.97
42	2.95	8.22	23.81
43	-5.82	-1.88	-10.20
44	-2.07	0.31	-0.67
45	-3.29	1.37	25.78
46	2.57	2.81	3.19
47	-5.15	7.72	-5.94
48	-2.63	-5.05	-6.12
49	2.52	0.99	1.81
50	1.72	2.66	-21.24
51	1.35	0.22	11.27
52	-1.48	-3.32	-22.03
53	-0.92	6.53	-0.86
54	0.96	7.22	4.88
55	-0.32	7.53	-6.17
56	-0.95	-5.36	-14.82

Table S2. Chemical shift reference correction (ε) and temperature difference (ΔT) for measurements made using the static, cryogenic probe and the MAS probe.

	ΔT (ºC)[a]	ε (ppb)
K19AV42ED47K	0.45	40.5
K19ED40NV42E	1.30	-23.7
K4AK19EV42E-C-His_6	0.74	-34.2
K4AK19EV42E-N-His_6	0.75	-36.2
T11KK19AV42E	0.60	69.6
K4AK19EV42E	0.57	-37.3

[a] $\Delta T = T_{MAS} - T_{cryoprobe}$.

Table S3. Parameters of the best-fitted residue-specific ^{15}N CSA tensors

Residue	Δσ (ppm)	Δσ error (ppm)	η	η error	β (°)	β error (°)
3	-159	2.0	0.42	0.03	19.5	0.6
4	-166	2.2	0.35	0.04	19.9	0.7
5	-166	1.8	0.20	0.02	17.9	0.5
6	-159	2.6	0.34	0.03	14.9	1.0
7	-164	1.7	0.26	0.03	19.4	0.6
8	-163	1.9	0.37	0.03	17.4	0.7
9	-159	2.1	0.39	0.02	25.9	0.5
16	-167	1.9	0.30	0.03	22.7	0.6
17	-164	2.0	0.19	0.04	22.1	0.6
18	-165	1.7	0.38	0.03	18.7	0.6
19	-151	1.8	0.44	0.04	16.1	0.5
21	-152	1.7	0.60	0.04	21.3	0.7
22	-181	1.8	-0.01	0.02	23.0	0.6
23	-159	1.6	0.62	0.05	17.5	0.4
24	-167	2.9	0.45	0.05	18.7	1.0
25	-177	2.0	0.06	0.05	20.4	0.8
26	-185	1.9	-0.02	0.03	20.1	0.7
27	-172	1.5	0.29	0.03	19.6	0.4
28	-171	2.6	0.33	0.05	19.3	0.7
29	-176	1.9	0.19	0.04	18.8	0.8
30	-162	3.2	0.12	0.04	20.0	0.7
31	-181	1.4	0.16	0.03	20.7	0.4
32	-174	2.2	0.23	0.04	18.7	0.6
33	-178	2.1	0.15	0.04	21.7	0.6
34	-175	1.5	0.35	0.04	18.5	0.5
35	-171	2.1	0.24	0.05	21.0	1.0
36	-175	1.7	0.11	0.04	21.6	0.6
37	-161	2.4	-0.01	0.03	24.3	0.7
38	-167	1.5	-0.06	0.03	20.1	0.6
39	-148	3.2	0.18	0.05	15.8	0.8
42	-150	4.2	0.60	0.02	15.7	1.0
43	-164	1.7	0.20	0.03	21.1	0.5
44	-167	1.7	0.35	0.03	21.2	0.5
45	-154	2.0	0.30	0.02	17.9	0.7
46	-162	2.0	0.17	0.04	17.3	1.0
47	-158	1.8	0.36	0.04	20.1	0.5
49	-161	1.8	-0.13	0.02	23.8	0.5
50	-187	1.7	-0.10	0.02	22.1	0.8
51	-165	1.9	0.21	0.03	20.5	0.7
52	-171	1.9	0.17	0.03	21.4	0.5
53	-159	2.3	0.30	0.02	20.3	0.7
54	-173	1.8	0.28	0.03	14.3	0.7
55	-161	1.8	0.30	0.02	16.8	0.8
56	-166	1.8	0.38	0.03	16.3	0.5

Table S4. Measured RCSA (ppb) for six mutants after temperature correction. The error in the RCSA is estimated at 5 ppb.

Residue	K19AV42E D47K	K19ED40N V42E	K4AK19E V42E-C-His_6	K4AK19E V42E-N-His_6	T11KK19A V42E	K4AK19E V42E
3	-154.1	-73.8	-14.6	-59.6	-95.5	-22.6
4	5.0	-106.9	-61.8	-107.4	-83.3	-84.1
5	-56.9	-3.3	-17.6	-45.9	62.9	-18.1
6	-39.9	-39.8	-1.7	-81.7	-61.8	-18.1
7	-9.4	63.0	-8.9	-30.0	82.2	-4.8
8	-72.8	28.9	47.3	-28.7	-66.3	47.7
9	85.7	82.6	-10.8	46.1	156.0	-4.6
10	-161.5	37.3	N/A	-32.6	-96.9	67.3
11	-80.0	-2.5	N/A	-40.4	-47.3	23.9
12	-7.0	9.6	-31.3	-57.9	45.4	-34.2
13	-28.3	-110.7	-44.0	-83.6	-76.7	-61.7
14	-86.3	-13.6	-19.6	-61.2	25.9	-31.3
15	-65.1	-79.1	-29.4	-121.6	-99.4	-58.1
16	-98.7	-72.6	-42.4	-84.9	-25.5	-53.5
17	1.8	-125.3	-70.0	-109.7	-98.7	-89.2
18	-122.7	-54.7	-46.5	-104.3	-142.9	-45.5
19	20.4	-81.7	-79.5	-103.8	-116.8	-100.4
20	-58.0	70.2	5.6	-66.0	-91.4	2.4
21	85.7	-51.5	-77.8	-58.2	-70.5	-91.9
22	-11.7	-135.9	-72.8	-107.1	-132.4	-98.9
23	151.4	-46.3	-32.1	16.3	-3.7	-46.7
24	226.9	N/A	-48.6	74.6	66.6	-59.9
25	134.3	N/A	-65.6	-54.7	-57.2	-94.1
26	113.9	-103.1	-36.7	-11.5	-34.2	-69.3
27	190.6	-19.9	-8.6	87.0	55.4	-21.7
28	224.0	-52.8	-57.5	46.3	53.3	-75.7
29	107.3	-93.6	-53.3	-29.1	-68.0	-79.0
30	130.6	-40.6	-0.9	64.9	33.1	-14.6
31	214.0	4.8	-2.6	144.4	105.8	-5.3
32	218.3	-50.8	-56.5	36.9	37.6	-80.7
33	102.1	-82.1	-23.8	19.0	-23.5	-39.5
34	157.7	-5.6	17.5	111.1	63.0	6.0
35	240.6	-32.2	-29.0	104.5	87.8	-44.4
36	152.1	-75.0	-49.6	-4.6	-26.2	-74.6
37	32.0	-61.9	-16.8	1.3	-19.5	-13.7
38	-30.5	57.1	84.0	137.0	53.7	98.9
39	-66.9	16.2	47.7	100.0	62.9	54.2
40	-9.2	8.6	63.0	42.0	-18.0	58.1
41	-85.0	44.1	65.2	62.2	8.7	68.4
42	-20.4	37.7	66.8	51.4	5.3	70.6
43	16.5	70.8	-8.7	-31.4	66.2	-7.9
44	-73.3	-106.1	-42.3	-112.3	-97.6	-59.9
45	-84.7	-24.4	-19.1	-37.6	43.2	-17.6
46	-64.3	-122.2	-57.6	-107.7	-107.3	-76.2
47	-5.4	5.5	-10.6	28.1	101.8	-0.4
48	145.0	57.0	-1.9	122.3	217.9	-4.2
49	16.8	28.2	-19.0	-19.2	103.8	-15.1
50	-106.2	-122.9	-62.2	-144.7	-136.3	-81.4

51	-14.5	-123.8	-73.3	-124.6	-133.8	-98.8
52	-35.9	0.6	-9.9	-11.6	87.7	-15.0
53	-58.5	-39.8	1.0	-81.2	-84.9	-11.0
54	-63.9	40.2	-3.3	-70.7	29.9	-1.8
55	-70.1	11.8	31.4	-51.2	-76.3	31.8
56	-32.1	82.7	-7.5	-53.9	47.9	4.2

Table S5. Measured relaxation rates (s^{-1}).[a] The estimated errors (used to determine weight factors during the fitting procedure) are 0.05, 0.02, 0.018, 0.018, 0.10 s^{-1} respectively.

Residue	$\Gamma^{CSA,NH}$ [b]	$\Gamma^{CSA,NC'}$ [c]	R_1 (600)[d]	R_1 (800)[e]	R_2 (600)[f]
3	3.16	-0.33	1.05	0.86	2.71
4	3.50	-0.40	1.04	0.86	3.62
5	3.43	-0.33	1.07	0.90	3.10
6	3.56	-0.31	N/A	0.85	N/A
7	3.33	-0.33	1.04	0.87	3.30
8	3.57	-0.29	1.04	0.88	5.53
9	2.79	-0.32	0.98	0.82	3.16
10	3.20	-0.34	N/A	N/A	N/A
11	2.83	-0.21	N/A	N/A	N/A
12	2.69	-0.26	N/A	N/A	N/A
13	2.98	-0.30	N/A	N/A	N/A
14	2.50	-0.39	N/A	N/A	N/A
15	2.87	-0.34	N/A	N/A	N/A
16	3.10	-0.33	1.05	0.89	5.87
17	3.19	-0.30	1.01	0.84	4.98
18	3.21	-0.38	1.05	0.88	3.46
19	3.35	-0.33	0.98	0.80	3.23
20	3.43	-0.29	N/A	N/A	N/A
21	3.03	-0.29	0.96	0.85	3.26
22	3.61	-0.27	1.11	0.94	3.62
23	3.66	-0.37	1.02	0.86	3.62
24	3.78	-0.32	1.03	0.84	3.68
25	3.85	-0.29	1.07	0.89	3.67
26	4.00	-0.48	1.12	0.95	4.26
27	3.95	-0.31	1.03	0.84	3.64
28	3.85	-0.33	1.04	0.85	3.69
29	3.93	-0.30	1.08	0.90	3.73
30	3.69	-0.35	N/A	N/A	N/A
31	4.12	-0.35	1.05	0.87	4.18
32	3.96	-0.33	N/A	N/A	N/A
33	3.87	-0.34	1.05	0.86	3.71
34	4.04	-0.34	1.08	0.89	3.95
35	3.81	-0.34	1.02	0.83	3.62
36	3.74	-0.33	1.05	0.86	3.85
37	3.22	-0.25	0.98	0.79	3.92
38	3.65	-0.24	1.03	0.85	3.87
39	3.54	-0.33	N/A	N/A	N/A
40	3.10	-0.27	0.95	0.81	3.14
41	2.04	-0.26	N/A	0.84	2.83
42	3.41	-0.32	N/A	N/A	N/A

43	3.25	-0.35	1.03	0.85	3.32
44	3.27	-0.33	1.05	0.88	3.30
45	3.15	-0.31	1.01	0.85	3.14
46	3.50	-0.26	N/A	0.88	N/A
47	3.19	-0.34	1.02	0.83	3.30
48	3.27	-0.29	1.04	0.87	3.61
49	3.07	-0.23	1.01	0.85	3.26
50	3.80	-0.22	1.16	1.01	3.93
51	3.28	-0.23	1.05	0.84	3.30
52	3.32	-0.32	1.09	0.92	3.60
53	3.26	-0.33	0.98	0.83	3.89
54	3.70	-0.32	1.14	0.98	5.21
55	3.54	-0.29	1.00	0.85	4.36
56	3.57	-0.33	1.07	0.92	3.47

[a] R_1 and R_2 values are for ^{15}N-{^{2}H} groups, measured in D_2O solvent.
[b] Transverse ^{15}N CSA/^{15}N-$^1H^N$ dipolar cross-correlated relaxation rates and
[c] Transverse ^{15}N CSA/N-C′ dipolar cross-correlated relaxation rates measured at 600 MHz field, 298K.
[d,e] Longitudinal (R_1) relaxation rate of ^{15}N-{^{2}H} measured at 283K in 100% D_2O, at 600[d] and 800[e] MHz ^{1}H frequency. Missing values (N/A) are due to very rapid relaxation, overlap of the ^{13}C-$^1H^a$ correlation of the preceding residue (used for readout), or insufficient exchange from ^{15}N-^{1}H to ^{15}N-^{2}H.
[f] Transverse (R_2) relaxation rate of ^{15}N-{^{2}H} measured at 283K in 100% D_2O, at 600 MHz ^{1}H frequency.

Table S6. Average CSA tensor components and orientations in α-helical and β-strand conformations.[a]

	σ_{ZZ}	σ_{XX}	σ_{YY}	β (°)	γ_1 (°)	γ_2 (°)
α-helix[a]	-115.5±0.3	71.9±0.7	44.6±0.9	19.6±0.2	2.5±0.2	19.4 ±0.2
β-strand[a]	-108.8±0.3	70.8±0.6	37.9±0.5	19.1±0.1	0.6±0.3	19.1±0.1

[a.] Five parameters ($\Delta\sigma$, η, β, γ_1, γ_2) are utilized and assumed to be the same over all α-helix or all β-strand residues (Scheme S1). The uncertainty represents the spread obtained when adding estimated noise to experimental data in a Monte Carlo type analysis.

Table S7. Chemical shift tensors calculated for N-formyl-Ala-Ala with backbone torsion angles taken from various positions in GB3[a].

Residue[b]	δ_{ZZ} (ppm)	δ_{YY} (ppm)	δ_{XX} (ppm)	$\Delta\sigma$(ppm)	η
V21	220.4	113.5	30.5	-148.4	0.84
A23	217.2	112.8	28.7	-146.5	0.86
A26	219.0	97.0	30.2	-155.4	0.64
G38[c]	207.1	61.7	32.2	-160.2	0.28
K50	218.2	76.6	52.6	-153.6	0.23
T53	217.9	97.8	35.9	-151.1	0.62

[a] The chemical shift tensor is calculated by $\delta_{ii} = 244.6 - \sigma_{ii}$ where σ_{ii} is the calculated absolute shielding tensor

[b] The residue number corresponds to the second residue of the N-formyl-Ala-Ala dipeptide, and uses backbone angles taken from PDB entry 2OED

[c] The model for G38 is Ala-Gly instead of Ala-Ala

Table S8. Normalized (1.04 Å) N-H bond vectors relative to the heavy atoms of PDB entry 2OED, used in the ^{15}N CSA fitting.

Residue number	x coordinate (Å)	y coordinate (Å)	z coordinate (Å)
3	-0.880	0.318	-0.453
4	1.008	-0.245	0.074
5	-1.008	-0.179	0.186
6	0.927	-0.038	-0.471
7	-0.832	-0.388	0.489
8	0.658	0.066	-0.803
9	-0.856	-0.531	0.257
10	0.115	0.359	-0.969
11	0.233	-0.071	-1.011
12	0.862	0.380	-0.441
13	-0.985	0.080	0.323
14	1.016	0.058	-0.214
15	-1.014	-0.044	0.225
16	1.032	-0.036	-0.121
17	-1.006	0.215	-0.151
18	0.854	-0.460	0.375
19	-0.809	0.478	-0.446
20	0.412	-0.654	0.696
21	-0.513	0.596	-0.681
22	-0.668	0.797	0.001
23	0.747	-0.721	-0.060
24	0.462	-0.822	-0.439
25	0.325	-0.988	-0.028
26	0.682	-0.783	-0.049
27	0.664	-0.715	-0.362
28	0.296	-0.889	-0.452
29	0.470	-0.926	-0.065
30	0.677	-0.760	-0.214
31	0.450	-0.716	-0.606
32	0.172	-0.972	-0.328
33	0.486	-0.897	-0.201

34	0.627	-0.710	-0.429
35	0.286	-0.817	-0.576
36	0.278	-0.965	-0.271
37	0.804	-0.632	-0.189
38	0.070	-0.270	-1.002
39	-0.361	-0.683	-0.696
40	-0.161	0.466	0.916
41	0.155	-0.465	-0.917
42	-0.254	0.070	1.006
43	0.576	0.453	-0.738
44	-0.955	-0.058	0.407
45	1.021	0.132	-0.147
46	-1.037	0.081	0.006
47	0.967	0.371	-0.093
48	0.655	0.735	0.336
49	0.558	0.875	-0.074
50	1.021	-0.115	-0.159
51	0.999	-0.198	0.213
52	-1.024	-0.183	-0.029
53	0.910	0.074	-0.499
54	-0.840	-0.303	0.533
55	0.762	0.001	-0.708
56	-0.665	-0.446	0.664

(1) Spiess, H. W. *NMR, Basic Princip. Progr.* **1978**, *15*, 55-214.
(2) Wylie, B. J.; Sperling, L. J.; Frericks, H. L.; Shah, G. J.; Franks, W. T.; Rienstra, C. M. *J. Am. Chem. Soc.* **2007**, *129*, 5318-5319.
(3) Xu, J.; Millet, O.; Kay, L. E.; Skrynnikov, N. R. *J. Am. Chem. Soc.* **2005**, *127*, 3220-3229.
(4) Wang, A. C.; Bax, A. *J. Biomol. NMR* **1993**, *3*, 715-720.
(5) Ying, J. F.; Chill, J. H.; Louis, J. M.; Bax, A. *J. Biomol. NMR* **2007**, *37*, 195-204.
(6) Cornilescu, G.; Bax, A. *J. Am. Chem. Soc.* **2000**, *122*, 10143-10154.
(7) Orbons, L. P. M.; Vandermarel, G. A.; Vanboom, J. H.; Altona, C. *Eur. J. Biochem.* **1987**, *170*, 225-239.